Experimental Techniques
https://doi.org/10.1007/s40799-021-00458-0

RESEARCH PAPER

Application of the Hough Transform for Automated Analysis of Kolsky Bar Data

S.-D. Salehi[1] · W. Gilliland[1] · O.T. Kingstedt[1]

Received: 18 September 2020 / Accepted: 1 March 2021

Abstract

The Kolsky Bar, also known as the split-Hopkinson pressure bar, has become one of the most commonly used apparatuses when studying the dynamic behavior of materials. Despite its popularity, limited standards exists with respect to the design, data collection, and data analysis approach used. A lack of standardization can lead to lab-to-lab variation in reported dynamic behavior for nominally identical materials. A key step during data reduction is the appropriate selection of the signal windows used in the one-dimensional wave propagation analysis of recorded strain gauge signals. The presented work provides an automated analysis approach for selecting signal windows based on the Hough transform. The approach is agnostic to loading mode (e.g., tension vs. compression), applicable to both pulse-shaped and non-pulse shaped experiments, robust in the presence of naturally occurring signal oscillations and noise, and has rapid computation time. Two cases are selected to demonstrate the viability of applying the Hough transform to recorded Kolsky bar signals. In the first case, the bar wave speeds of maraging steel tension and compression Kolsky bars are determined. The second case demonstrates the application of the Hough transform technique in the study of the dynamic compression behavior of additively manufactured Inconel 718. A stress-strain curve generated using the automated HT-based technique is compared to those determined manually showing the automated approach provides a closely matching result. Window selection automation provides an important step toward improving consistency of results reported, data processing throughput, and traceability of dynamic mechanical property data generation.

Keywords Split-Hopkinson pressure bar · Kolsky bar · Dynamic behavior of materials · Hough transform

Introduction

The Hough transform (HT) was initially created and patented by Paul Hough [1]. Its development was motivated by the need to identify curves in binary bubble chamber images [2]. The HT converts a feature detection problem (e.g., finding straight lines) from the (x, y) image space to a peak detection problem in a user defined parameter space. The original parameter space selected was the slope-intercept (m, c) space. The (m, c) parameter space has a noticeable limitation in that it is unable to parameterize vertical lines (i.e., $m \rightarrow \infty$). As Duda and Hart [3] pointed out, the distance-orientation angle (ρ, θ) parameter space overcomes this limitation while also simplifying computation.

The identification of straight lines (or line segments) is the most commonly used application of the HT. One such example is the identification of Kikuchi bands [4, 5] in images recorded during electron backscatter diffraction crystal orientation mapping. Another application of linear Hough transform is the determination of the fiber orientation distribution in non-wovens [6, 7]. In the (ρ, θ) parameter space, the position of points in a binary image (i.e., those with an intensity of 1) can be defined by their distance (ρ) and angular orientation (θ) from the image origin (e.g., bottom left corner), see equation (1).

$$\rho = x\cos(\theta) + y\sin(\theta) \tag{1}$$

In practice, equation (1) is solved at each point in the binary image at user defined intervals of θ where $\theta \in (0, \pi)$. Using this approach, each point (Fig. 1(a)) is represented by a sinusoidal line (Fig. 1(b)) in the (ρ, θ) space. The intersection of the collection of sinusoidal lines gives the

✉ O.T. Kingstedt
o.kingstedt@utah.edu

[1] Department of Mechanical Engineering, University of Utah, Salt Lake City, UT, 84112, USA

Published online: 02 April 2021

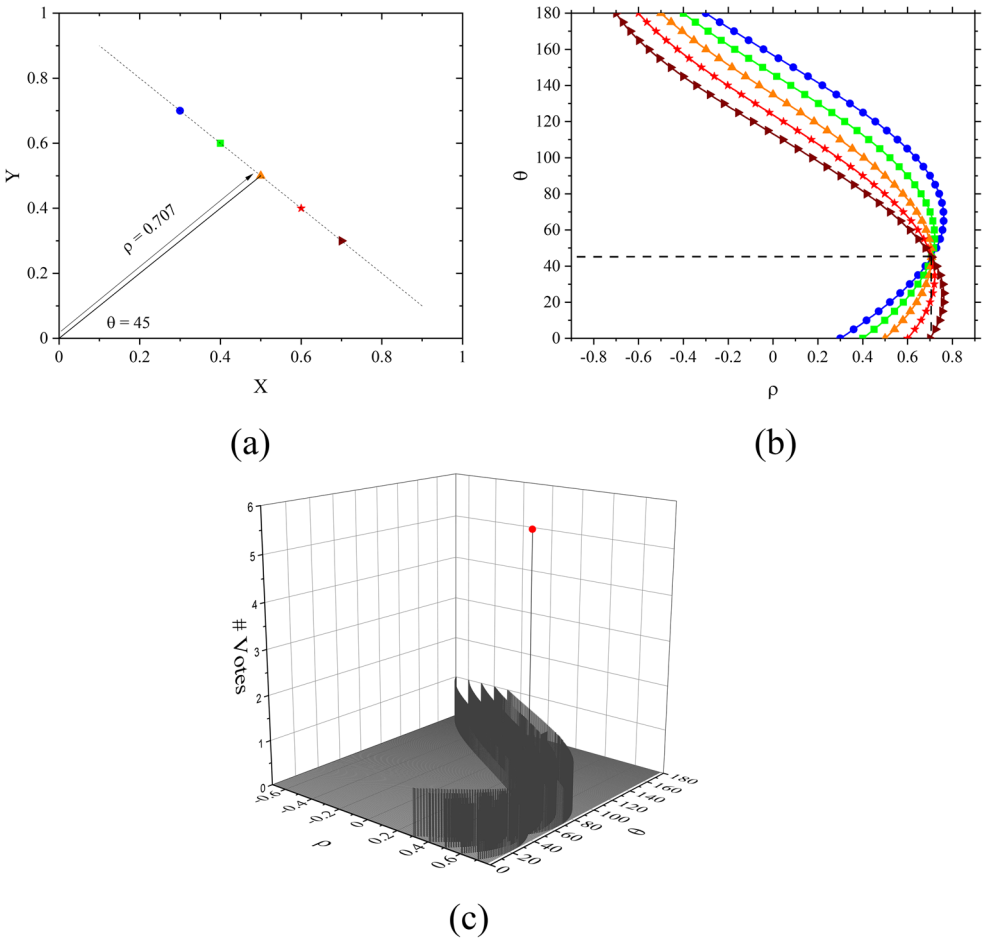

Fig. 1 An overview of HT straight line detection **a**) a set of colored points in (x, y) image space, **b**) sinusoidal lines in (ρ, θ) space whose coloring corresponds with the point coloring in a), c) accumulator of **b**) defining the ρ and θ of the co-linear points in **a**)

distance (ρ) and angular orientation (θ) of the straight line upon which the points in the original binary image are positioned. To automate selecting the intersection point of the sinusoidal lines, an accumulator of the ρ-θ parameter space is implemented (Fig. 1(c)). The accumulator counts the number of lines present with a user defined binning resolution. If only one line is present in the binary image, as in Fig. 1(a), the maximum value (i.e., peak) of the accumulator yields the ρ and θ values defining the straight line connecting points (see Fig. 1(c)). The amplitude of the peak in the accumulator space is a function of several factors including the number of points composing the line, the number of other points in the image and the choice of the bin size in the accumulator space. If there are multiple lines in an image a voting process is implemented to appropriately select the line feature(s) of interest. The voting process efficiency and robustness can be improved by limiting the accumulator space considered based on knowledge of the HT application area. Discussions in subsequent sections will be limited to the application of the HT to Kolsky bar data. For a more complete overview of the HT the reader is encouraged to consult the following review articles, refs [8–10].

In addition to line detection, the HT can be extended to identify other predefined objects in binary images such as, circular arcs [11], parabolas and ellipses [12–14], as well as arbitrary image shapes [15, 16]. Duda and Hart were the first to present the detection of circles [3], the circular Hough transform (CHT), using a modification of the linear Hough transform (LHT). The CHT finds circles characterized by a center point (x_0, y_0) and radius r. Shown in Fig. 2, is a set of colored points positioned on the circumference of the same black dashed circle. The CHT maps the colored points onto a 3-D cone shaped manifold (see Fig. 2); equation (2) presents the potential circles that form the manifolds. To determine the circle on which the colored points of interest exist, votes are accumulated in the 3-D parameter space (x_0, y_0, r). Equation (2) presents the potential circles that form the 3-D accumulator space. For each radius considered, there is a corresponding accumulator space. The voting procedure searches the accumulator space to determine the x_0, y_0, r value that yields the greatest peak and thus the circle that the colored points are positioned on. The voting procedure is illustrated in Fig. 2(b). Within Fig. 2, it is apparent that the radius of 1 results in the greatest number of intersections of the manifolds. The

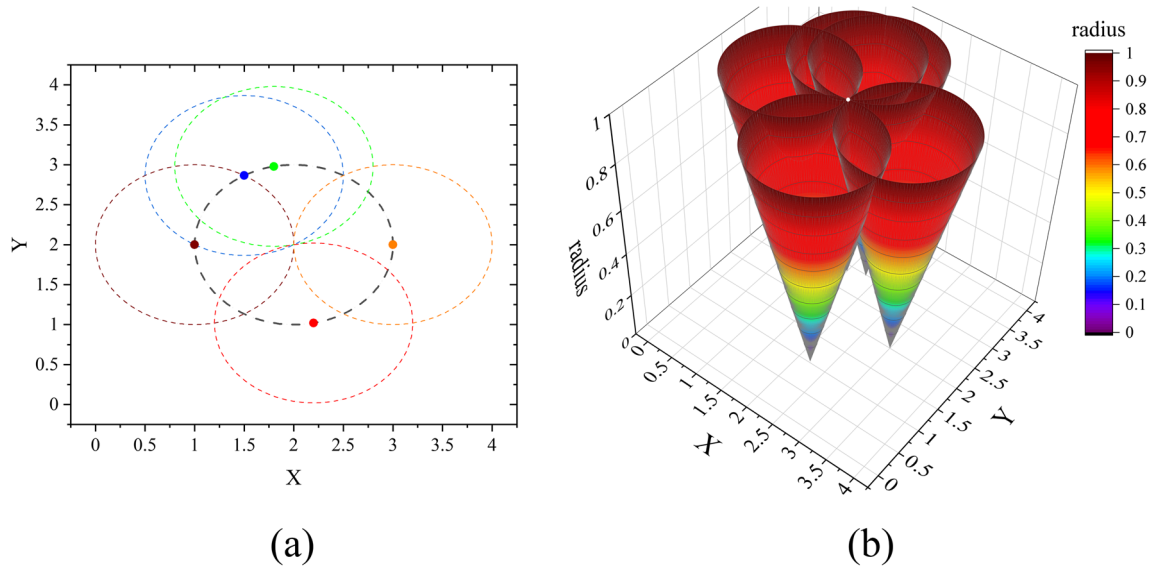

Fig. 2 Detection of a circle center using the circular Hough transform **a**) a set of colored points positioned on the same black dashed circle **b**) 3-D cone manifolds generated during the voting process. The white point indicates the position of the greatest number of manifold intersections which defines the center (x_0, y_0) of the detected circle

white point placed where the greatest number of manifold intersections occurs defines the (x_0, y_0) circle center. For any accumulator whose radius value is above or below 1, the number of manifold intersections would be lower. The CHT can also detect arcs in images which is analogous to the automated circle detection approach [17, 18].

$$r^2 = (x - x_0)^2 + (y - y_0)^2 \tag{2}$$

The Kolsky bar [19] is the most widely used experimental apparatus for studying the high-strain-rate ($\dot{\varepsilon} > 10^2 s^{-1}$) mechanical behavior of materials. The Kolsky bar can be configured to perform compression [19], tension [20, 21], shear [22], and torsion [23] experiments. The simplest and most commonly used version of the Kolsky bar is the compression configuration. The design of the specimen for a compressive Kolsky test is a critical component of the experiment. A robust specimen design procedure should satisfy three conditions: a) Inertia and friction effects should be absent to assure uniform deformation of the specimen; b) the specimen should achieve stress equilibrium; c) uniaxial stress condition should be achieved [24]. Gray [25] suggested the frictional and inertial effects could be decreased by reducing the areal mismatch between the bar and the specimen. Davies and Hunter [26] also suggested thickness to diameter ratio of the specimen to be between 0.5 and 1 based on the corrections for longitudinal and radial inertia effects.

There are many possible designs of the Kolsky bar apparatus that meet the specimen and apparatus geometry guidelines required for one-dimensional wave propagation assumptions to be valid [27]. These geometric requirements include length-to-diameter ratio of more than 20, perfectly aligned bars and low friction to allow bars to move freely. In addition, the incident and transmission bar lengths should be at least twice the striker length to avoid incident and reflected waves overlapping. These requirements do not require the apparatus to meet a specific size which enables the same one-dimensional wave propagation theory to be applied to micro-Kolsky bars [28] with diameters on the order of 1.59 mm with a total length of 47.6 mm, to systems with diameters of 100mm (e.g., [29]), or those that are tens of meters in length [30]. In addition to variations in the physical size of the Kolsky bar apparatus, experiment execution differences between laboratories include the use of pulse shaping, bar material, dispersion correction implementation, sampling rate, loading duration, and data acquisition bandwidth. Ultimately, the individualized nature of Kolsky bar testing can result in lab-to-lab variability in reported stress-strain behavior of nominally identical materials. One pathway to reduced variability in reported material behavior is to homogenize approaches implemented during data analysis, specifically methodologies used when selecting the incident, reflected and transmitted signal windows. As has been pointed out previously by Chen and Song [27], correct selection of the signal windows is critical to ensuring accurate results are reported.

The objective of the current study is to demonstrate an automated selection process of the incident, reflected, and transmitted signal windows that is agnostic to metallic bar material, bar geometry (i.e., length and diameter), and pulse shape. The automated selection process is founded

on the early developments of the HT. The HT method is selected due to it having a number of desirable features: 1) each data point is treated independently and thus parallel processing can be implemented resulting in nearly instantaneous calculation times; 2) data independence also enables the technique to recognize incomplete or deformed shapes which enable the technique to be applied to data sets captured at different sampling rates, as well as both pulse-shaped and non-pulse shaped experiments; 3) the HT is robust to the addition of noise, a common feature in experimental data. The automation of high-strain-rate experiment data analysis provides an important step forward in improving consistency of results reported, throughput, and traceability of mechanical property data generation.

Methodology

Description of the SHPB

As mentioned previously, there are many valid designs of the Kolsky bar that meet the requirements of one-dimensional wave propagation assumptions. The following discussion is limited to the compression Kolsky bar as it is the most common configuration. Regardless of its design, the apparatus typically consists of three long cylindrical bars, the striker bar (or tube), incident bar and the transmission bar, see Fig. 3. The incident pulse in compression Kolsky bar experiments is initiated when the striker bar impacts the incident bar. The striker bar is typically made from the same material and is the same diameter as the incident and transmitted bars. However there have been studies which use specialized (i.e., non-cylindrical) striker bars (e.g., [31]). The striker bar separates from the incident bar once the initial compressive wave has reflected as a tensile wave and reaches the striker bar incident bar interface (see the x-t diagram in Fig. 3). As a result, the pulse's spatial length is twice the striker's spatial length. The pulse amplitude is proportional to the striker's impact velocity which typically is controlled by adjusting the gas gun pressure used to launch the striker bar [32].

When the compressive pulse reaches the specimen, due to acoustic impedance, part of the wave is reflected towards the striker bar incident bar interface, and part of it is transmitted into the specimen. An additional reflection and transmission occurs as the propagating pulse reaches the specimen transmission bar interface. Strain gauges are mounted to the surface of the incident and transmission bar surfaces to record: 1) the incident pulse (ε_I) generated by the striker bar 2) the reflected pulse (ε_R) from the incident bar/specimen interface, and 3) the transmitted pulse (ε_T) in the transmission bar. Assuming one-dimensional wave propagation, these pulses can be used to determine the nominal engineering stress, strain, and strain-rate of the specimen using the following relationships.

$$\sigma_s(t) = \frac{E_{bar} A_{bar}}{A_{spec}} \varepsilon_{T(t)}, \tag{3}$$

$$\dot{\varepsilon}(t) = \frac{c_{bar}}{L_{spec}} (-2\varepsilon_{R(t)}), \tag{4}$$

$$\varepsilon_s = \int_0^t \dot{\varepsilon}(\tau) d\tau \tag{5}$$

In equations (3)-(5), E_{bar} is the elastic modulus of the bar material, A_{bar} and A_{spec} represent the cross-sectional area of the bar and specimen, respectively; L_{spec} is the specimen thickness, and c_{bar} is the wave speed in the incident and transmitted bars. The above relationships are valid once a balance (i.e., equilibrium) is achieved between the forces

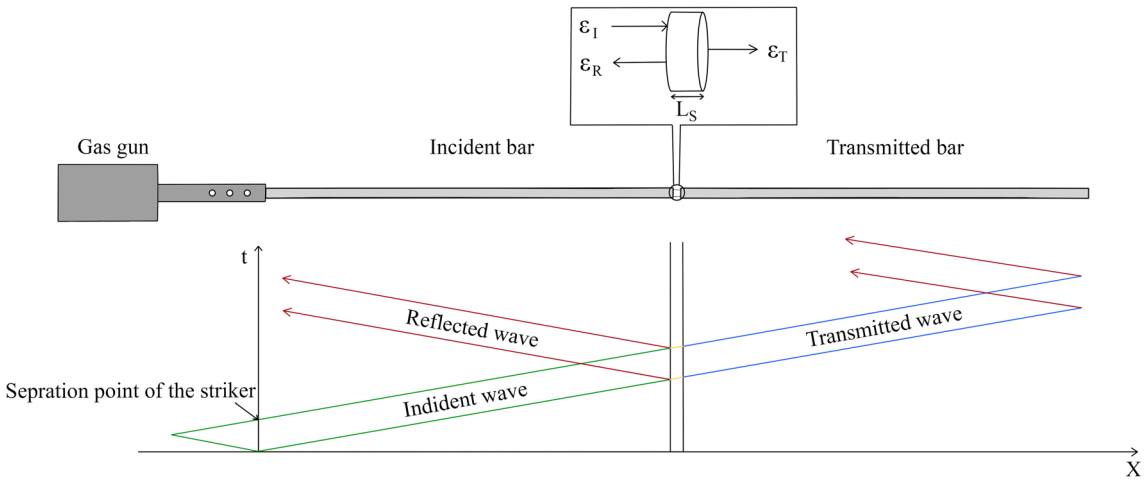

Fig. 3 Setup of the SHPB experiment with a Lagrangian x-t diagram of the wave propagation process

on either side of the specimen. The forces at the incident bar/specimen P_{inc} and specimen transmission bar P_{trans} interfaces are,

$$P_{inc} = A_{bar} E_{bar} (\varepsilon_I + \varepsilon_R) \tag{6}$$

$$P_{trans} = A_{bar} E_{bar} \varepsilon_T \tag{7}$$

In equations (3)-(7), the $\varepsilon_I, \varepsilon_R$ and ε_T pulse windows used must be selected from the recorded data set. The selection of these windows typically requires human input, as experiment-to-experiment variation of their positioning occurs due to the Kolsky bar being an open-feedback-loop apparatus. Window selection is an integral step during the reduction of strain gauge data to the specimen's stress-strain behavior. The primary contribution of the current work is the automation of accurate window selection.

Application of the Hough Transform

The following outlines two HT-based methodologies that can be used to fully automate Kolsky bar analysis. The first is based on the linear Hough transform (LHT) and the second uses the CHT. Kolsky bar data has a common structure consisting of incident, reflected, and transmitted pulses regardless of the material tested, bar geometry and loading mode (e.g., tension vs. compression).

Linear Hough Transform

Figure 4 provides an overview of the process used to identify the pulse windows using the LHT. An oscillation heavy signal is shown in Fig. 4(a) and is selected to demonstrate

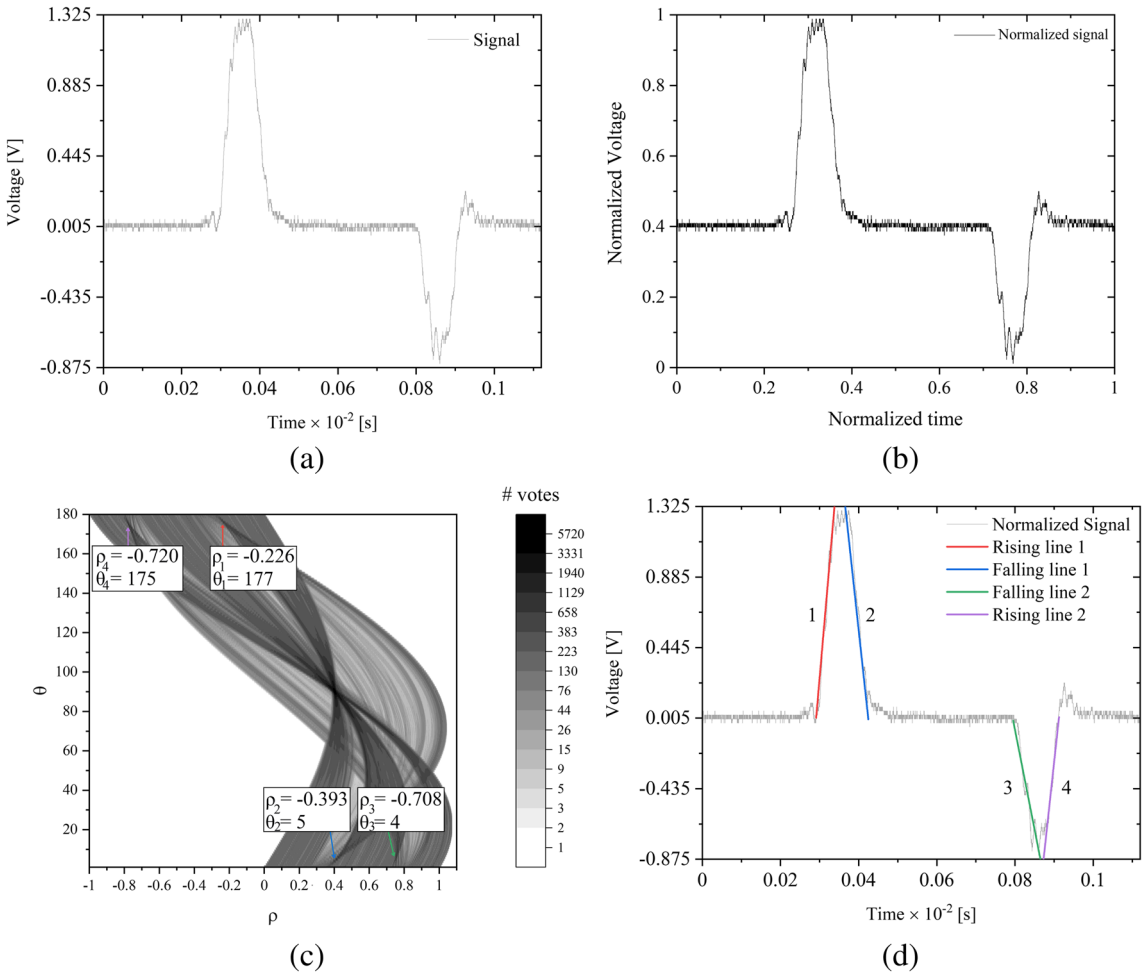

Fig. 4 Overview of the LHT applied to Kolsky bar data. **a**) A recorded Kolsky bar signal containing oscillations and noise. **b**) An amplitude and time normalized Kolsky bar signal with interpolated data points added in the vertical direction. **c**) The ρ, θ parameter Hough space of the Kolsky bar signal with the location of four peaks of interest indicated by colored arrows. **d**) The Kolsky bar signal with the rising and falling slopes of the incident and reflected signals determined from the accumulator space. Colors of the identified slopes correspond with the arrows identifying peaks in c)

the robustness of the HT both to noise and the natural signal oscillations recorded by the surface mounted strain gauges caused by three-dimensional wave propagation. The incident bar signal is used to demonstrate the technique as it is the more complex application of the HT due to having two pulse windows of interest, the incident and reflected pulses, while the transmission bar only has one window of interest, the transmitted pulse. To identify the window bounds of the incident and reflected pulses a total for two rising slopes and two falling slopes need to be identified in the Kolsky bar signal. The HT is intended for applications where sampling occurs over a square grid. Thus, the recorded Kolsky bar data discretization in the vertical direction must to be increased to match the time sampling rate of the experiment. The purpose of this step is to improve the robustness of the subsequent voting process. Without taking this step, short rise time features may be sampled by too few points to be identified during voting. The additional points are not considered after the voting process (i.e., they are not included in any of the one-dimensional wave analysis calculations used to obtain material behavior).

The first step of applying the HT to Kolsky bar data is to fit an interpolating spline to the recorded data set and interpolate data points so the Kolsky bar signal is "sampled" over even spacing in amplitude and time, see Fig. 4(a) axes. Next the signal is normalized in time and amplitude, see Fig. 4(b). After normalizing, each point is sampled in the ρ, θ space generating a large number of sinusoidal lines that form the accumulator space, see Fig. 4(c). In the accumulator space there are a number of peaks present with varying amplitudes. To remove the effects of noise, a threshold is set to remove small amplitude peaks corresponding to short line segments caused by noise or natural signal oscillations.

After thresholding, a total of five predominant peaks remain in the accumulator space. Among these, the peak with the greatest amplitude, located at $\rho \approx 0.4$ and $\theta \approx 90$, is attributed to the zero-slope quiescent periods in the signal. As will be discussed later, this peak is omitted from the voting procedure as it does not provide meaningful information for identifying the position of the incident or reflected signals. Peaks having negative radius and $\theta \in (\pi/2, \pi)$ corresponding to rising slopes, and those with positive radius and $\theta \in (0, \pi/2)$ correspond to falling slopes. Herein a positive radius is defined as having a positive vertical coordinate and a negative radius is defined as having a negative vertical coordinate. With the origin of the normalized data positioned at the bottom left corner, the increasing absolute ρ amplitude for peaks provides the ordering of the slopes in time for the signal shown in Fig. 4(c). The accumulator space shown can be interpreted as indicating four lines with non-zero slope, ordered such that there is a rising slope (red arrow), then a falling slope (blue arrow), followed by a falling slope (green arrow) and then a rising slope (purple arrow). The ρ, θ values corresponding to the four peaks shown in the accumulator space are then unnormalized. The lines predicted by the HT are then overlayed with the recorded data set, see Fig. 4(d).

Voting Process - Accumulator Space Reduction

The Hough transform accumulator process can be represented as equation (8). In this equation, $I(x, y)$ is equal to one for the data points in the normalized amplitude-time plane and equals zero for other points. $\delta()$ is the Dirac δ-function and $H(\rho, \theta)$ acts as the accumulator; therefore, the dominant lines in the signal possess larger H values (i.e., votes). After computing the H values for all possible lines in the digitized normalized space, there is a voting step to choose the best fit for all rising and falling lines.

$$H(\rho, \theta) = \int_{-\infty}^{\infty} \int_{-\infty}^{\infty} I(x, y)\delta(\rho - x\cos\theta - y\sin\theta)dxdy \tag{8}$$

To improve calculation times and prevent the selection of the peak corresponding to the quiescent periods of the recorded data set, only specific locations in the Hough space need to be searched for the rising and falling slopes of the incident and reflected pulses. As it can be seen in Fig. 5, in the typical normalized signal of the Kolsky bar experiment, the first rise and fall of the signal are located at the top and bottom of the accumulator space respectively, and have an absolute radius value less than half; see boxed regions labeled 1 and 2. Therefore, equations (9), (10) present the sets (c_1, c_2) that contain the peaks related to the first rise and fall. The maximum values of these sets correspond to the selected rising and falling lines. The intersections of these lines with the time-axis of the recorded signal determines the boundary points of the respective pulse windows. The subsequent windows that contain the reflected and transmitted pulses should have the same width as the incident signal. Consequently, once the first window is determined using the HT, the remaining windows can be selected by finding their leading edge and setting their width to match the incident signal window. The LHT is particularly useful when applied to signals that have uniform rising and falling slopes.

$$c_1 = \left\{ H(\rho, \theta) \middle| |\rho| < 0.5, \rho < 0, 180 - c < \theta < 180 \right\} \tag{9}$$

$$c_2 = \left\{ H(\rho, \theta) \middle| |\rho| < 0.5, \rho > 0, 0 < \theta < c \right\} \tag{10}$$

Circular Hough Transform

In cases where pulse shaping is used, the initial portion of the signal rise can be shallow enough that alternative

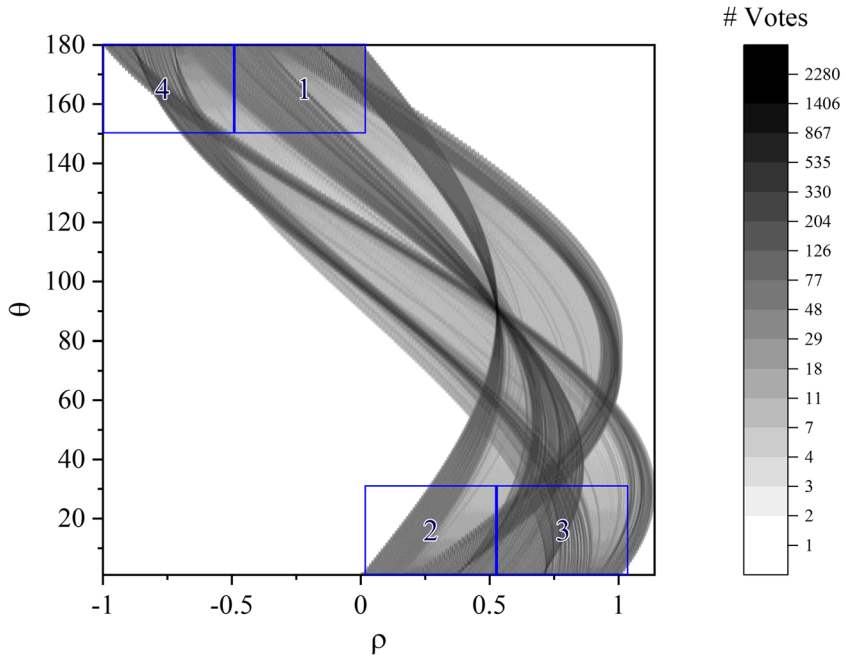

Fig. 5 The locations of the rising and falling lines in the accumulator space

approaches must be implemented to capture the beginning and end of signal windows correctly.

An example of this case is shown in Fig. 6. To account for these curvatures in the analysis and include them in the identified pulse windows, the CHT can be employed to find the arc that best follows those curvatures. The accumulator of the CHT is provided in equation (11). In order for this formulation to provide accurate predictions, two constraints are imposed. These constraints are necessary due to the short arc lengths present at the pulse's leading and trailing edges which results in relatively small amplitude peaks in the accumulator space. The first constraint requires the predicted circle to be tangent to the rising (or falling) slope found by the LHT and the adjacent quiescent portion of the signal. This first constraint requires the peak found in the accumulator space to be positioned correctly. For the incident and transmitted pulses it requires the fitting circle to be above the quiescent region of the signal. This constraint is graphically presented for the rising edge of the in Fig. 7. For the reflected signal, it requires the circle to be below the quiescent region of the signal. Additional constraints are to inform the central angle of the arc used to the voting space to be similar to the angle of the rising (or falling) slope, and to limit the allowable circle radius to be less than 0.2. Theoretically, the maximum allowable radius is close to 1, due to the normalized voltage-time

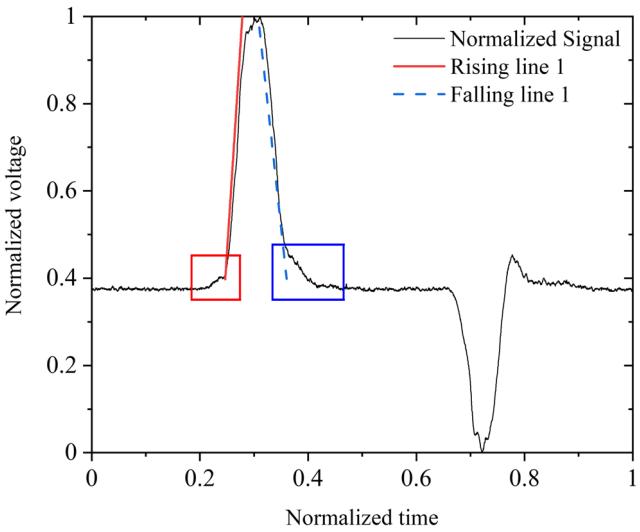

Fig. 6 Boxed regions indicating the missed ascending and descending signal curvatures when applying the LHT to pulse shaped experiments

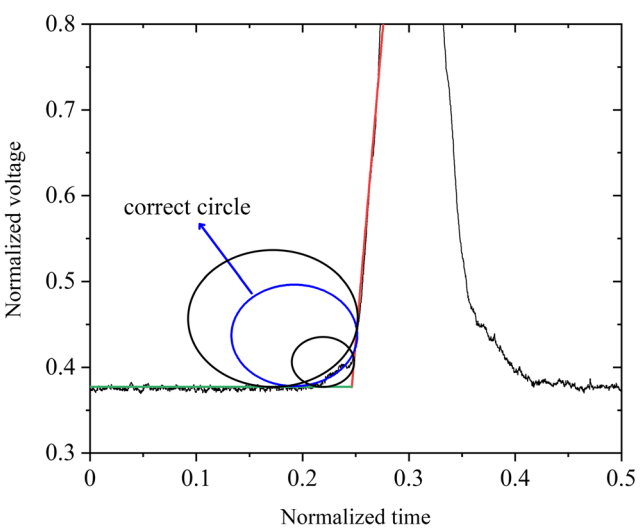

Fig. 7 Constraints of the detected arcs

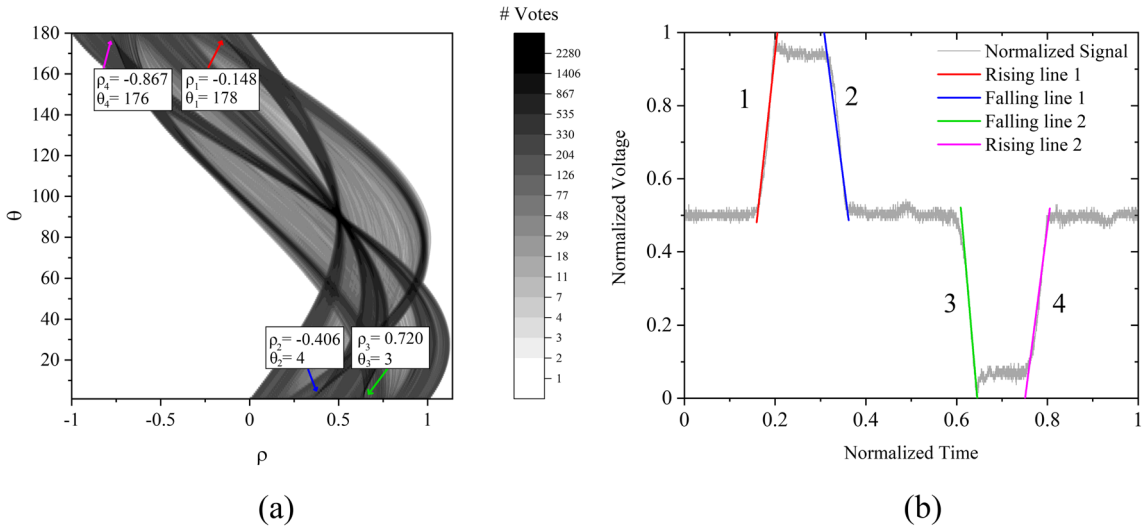

Fig. 8 **a**) The accumulator space of the tensile calibration experiment **b**) The rising and falling slopes detected in the tensile calibration experiment

space used. However, the choice to use a cut-off radius is founded on the CHT being used for arc detection opposed to the detection of a complete circle. The curvature of an arc is inversely proportional to its radius. Therefore, as the arc radii increases, its curvature decreases. This decrease in curvature results in inflated voting in the accumulator space for large radii arcs as their curvature more closely matches zero-curvature of the quiescent region. The signal rise and signal fall are treated independently as they can have different curvature characteristics. Once the circles with the best fit are determined, the position where they meet the tangent line of the quiescent portion of the signal is selected as a boundary point for the signal window. As with the LHT, once the temporal width of the incident signal is determined, it is used as the width for the reflected and transmitted signals. For the data shown, this assumption is valid since the signals shown here are pulse shaped and show limited dispersion. If pulse shaping is not used, a dispersion correction such as that proposed by Follansbee and Frantz [33], Li and Lambros [34], or Francis et al. [35], should be used to account for pulse length changes as the wave propagates.

$$H(x_0, y_0, r_0) = \int_{-\infty}^{\infty}\int_{-\infty}^{\infty}\int_{0}^{\infty} I(x, y)\delta((x-x_0)^2+(y-y_0)^2-r_0^2)dxdydr \tag{11}$$

Table 1 Comparison of bar wave speed predictions determined manually and using the LHT and CHT

	Compression Incident Bar Wave Speed (m/s)			Tension Incident Bar Wave Speed (m/s)		
Exp. No.	Manual	LHT	CHT	Manual	LHT	CHT
1	4946	4917	4921	4932	4996	5047
2	4930	4860	4806	4979	4938	5087
3	4906	4907	4908	4901	4907	4668
4	4917	4848	4900	5002	4927	5049
5	4995	4945	4854	4950	4874	4857
6	4925	4954	4900	4928	4907	5245
7	4961	4969	4851	4982	4920	5086
8	4926	4890	4954	4988	4929	5089
ine Avg. (m/s)	4938.2	4904.3	4886.7	4957.8	4924.7	5016.0
ine Std. Dev. (m/s)	28.5	45.9	46.8	35.3	34.8	175.7
% Difference from Human Selection	–	0.68	1.04	–	0.67	1.17

Results and Discussion

Two case studies are presented to demonstrate the automated data processing capabilities of the aforementioned HT-based signal window selection. In the first case study, the bar wave speed of a tension Kolsky bar and the bar wave speed of a compression Kolsky bar are determined. Both bars investigated are made from 350C maraging steel. The second case study demonstrates the ability to reduce raw compression Kolsky bar data to obtain the dynamic stress-strain behavior of additively manufactured Inconel 718.

Automated Wave Speed Calibration

The bar wave speed of a Kolsky bar apparatus must be known prior to conducting experiments. While textbook values of the bar material properties can be used to predict the bar wave speed, a direct measurement of the bars is preferable as an accurate understanding of the bar wave speed is required to calculate the specimen's nominal engineering stress-strain history. A direct measurement of the bar wave speed can be obtained by conducting an experiment without a specimen present and tracking the time necessary for the incident wave to reflect off the bar free surface and pass back over the mounted strain gauges.

A bar wave speed calibration experiment was conducted on the incident bar of a tension Kolsky bar (3658mm long, 19.05mm diameter), and on the incident bar of a compression Kolsky bar (2498 mm long, 19.05mm diameter). At the mid-length of the each incident bar a full Wheatstone bridge is mounted to the bar to observe the propagating pulses. Figure 8 presents the accumulator space, recorded signal and predicted rising and falling slopes of the incident and reflected waves of a nominal wave speed calibration experiment conducted on the tension

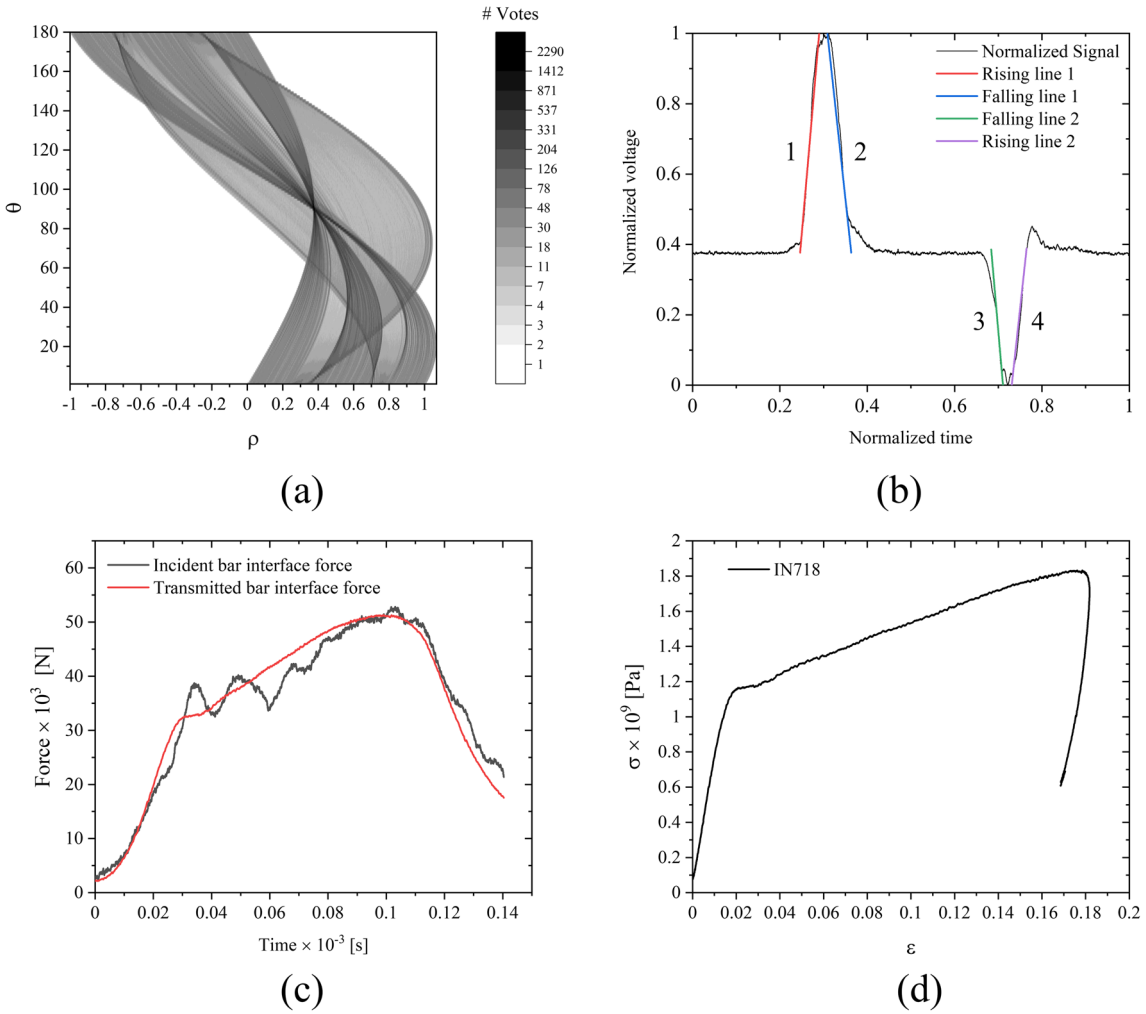

Fig. 9 **a**) The accumulator space of the incident signal. **b**) The detected lines in the signal **c**) Force-balance at the sides of the specimen d) Stress-strain behavior of the IN-718 specimen

incident bar. The accumulator space shown is generated using the approach outlined in "Linear Hough Transform" and "Voting Process - Accumulator Space Reduction".

After determining the intersections of the rising and falling slopes with the quiescent regions of the signal, the total wave propagation distance is used to determine the longitudinal bar wave speed. A total of eight nominally identical calibration experiments were conducted on each Kolsky bar. Table 1 presents the wave speeds found manually, and using the LHT and CHT approaches are presented in "Linear Hough Transform and "Circular Hough Transform", respectively. The textbook longitudinal wave speed for 350C maraging steel is, $c_{bar} = \sqrt{200GPa/8080kg/m^3} = 4969m/s$. The manual selection of the incident and reflected windows results in wave speed values that are close matches to the textbook value. Overall, the LHT and CHT predict average wave speeds that are in agreement to those found manually (i.e., within $\approx$ 1%). The positive agreement found between manually selected windows and the automated selection of windows indicates the promise of data automation applied to the Kolsky bar begin able to match that of experienced users. Examining

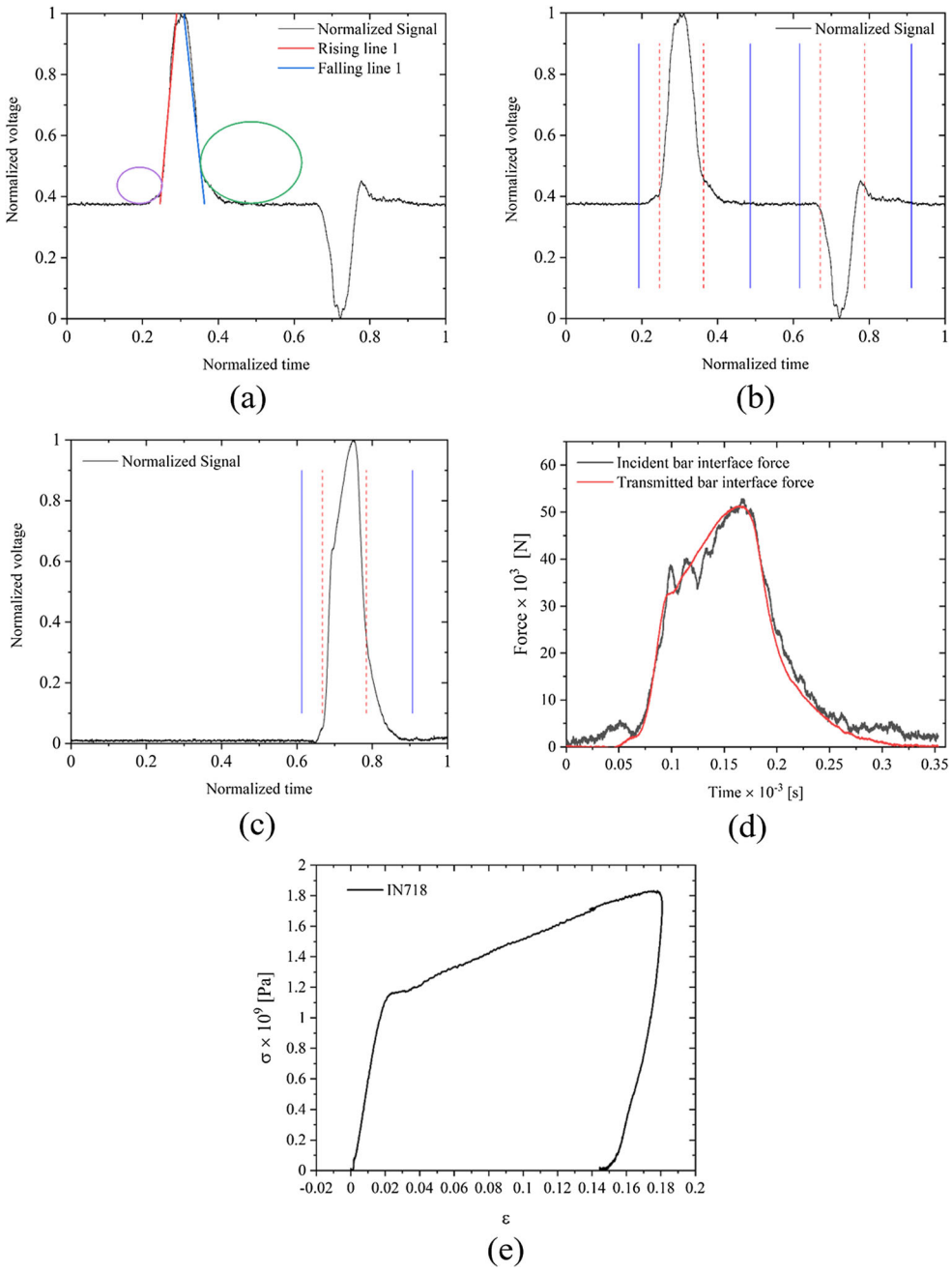

Fig. 10 **a**) Detected arcs and their location. **b**) A comparison of the pulse windows determined using the LHT (red dashed) and the CHT (blue solid) for the incident signal. **c**) A comparison of the LHT and CHT for the transmitted signal nalysis for **d**) Force-balance at the sides of the specimen as determined by the CHT **e**) Stress-strain behavior of the IN-718 specimen

the CHT predictions it is clear for the tension incident bar the standard deviation of predicted wave speeds is larger than for other data sets. Occasionally, the CHT will select a circle of best fit that is inaccurate, typically in the presence of noise. This is a known challenge with the CHT, with recent areas of investigation aimed at improving detection accuracy (e.g., [36–38]).

Test Case 2: Automated Compression Kolsky Bar Experiment Analysis

A dynamic compression experiment was conducted on a cylindrical additively manufactured Inconel 718 specimen, 3mm in length with 6mm diameter using a Kolsky bar consisting of a 203mm striker bar, 2489mm incident bar, and 1981mm transmitted bar all with 19mm diameters. Pulse-shaping was implemented using two copper discs 9.5mm in diameter 0.5mm thick. The motivation to include pulse shaping in the experiment is to prevent the use of the striker bar length to infer pulse duration.

The LHT transform was performed on the normalized signals from the Kolsky bar experiment. The accumulator space for the incident bar (i.e., the incident and reflected signals) is shown in Fig. 9(a), and the corresponding signals with LHT predicted slopes are provided in Fig. 9(b). Note, the sign of the compression Kolsky bar signal has been inverted for consistency of data presentation. Applying the LHT to the pulse-shaped signal leads to a few notable issues. It can be seen that the curvature at the beginning and end of signals is not properly included, particularly in the case of falling line 2 on the reflected pulse. However, the accurate prediction of the rise of the incident pulse enables automated data analysis to be executed if the wave speed from a calibration experiment is used to determine the reflected and transmitted pulse windows. Using these pulse windows the presence of a force balance is confirmed having occurred during the experiment, see Fig. 9(c). Knowing that a force balance is present, the resulting stress-strain behavior is calculated using equations (3)-(5). In Fig. 9, the stress-strain curve does not start at the origin. The cause of this is the LHT clipping the initial rise and thus the initial specimen behavior is not properly accounted for in the predicted stress-strain behavior.

To account for each signal's leading and trailing edge curvatures, the CHT was performed. Figure 10(a) shows the circles that determined to best match the curvature of the leading and trailing edge of the incident pulse. For comparison, the normalized Kolsky bar signal is shown in Fig. 10(b) and (c), for the incident and transmitted bar signals respectively, with overlaid lines indicated the analysis windows determined using the LHT (red dashed) and the CHT (blue). It is clear the CHT widens the pulse windows sufficiently to capture any leading and trailing edge curvature. The force balance using the CHT pulse windows is shown in Fig. 10(d) and the reduced stress-strain curve is presented in Fig. 10(e). Comparing the stress-strain curves of Figs. 9(e) and 10(e) it is apparent that the CHT more appropriately captures the entirety of the specimen deformation behavior, particularly at the earliest stages of deformation.

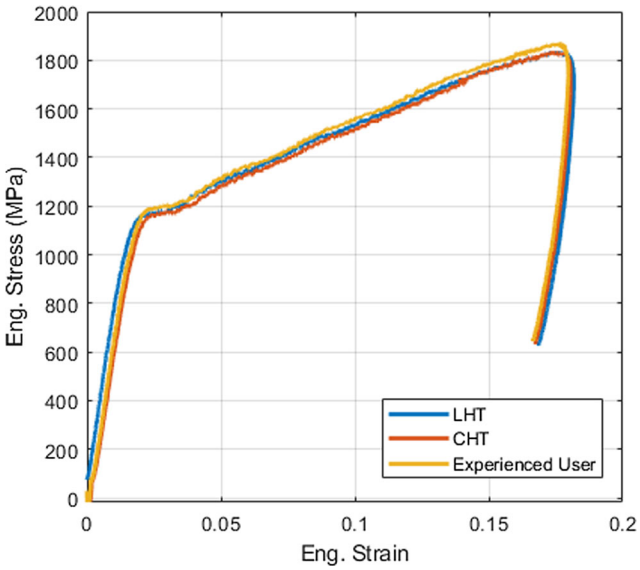

Fig. 11 Comparison of the LHT, CHT and human processed Kolsky bar data from the same experiment. A close match between the automated HT-based data analysis approach and experienced user processed data is evident

For the data set shown, the automated analysis using the LHT and CHT take 66 and 89 seconds to complete, respectively. The stress-strain curves using the LHT and CHT are compared to the stress strain curve obtained for the same data set processed manually by and experience user in Fig. 11. The CHT data and the experienced user data are nearly identical, giving evidence that the proposed CHT method is a viable methodology for automated data analysis.

Conclusions

The Hough transform has been widely adopted in the image processing community to automate the identification of linear and curved features of interest from binary images. The presented work leverages the HT to conduct fully automated data analysis of Kolsky bar signals. Two case studies were presented, demonstrating the window selection technique can be used during bar wave speed calibration, and can be used to determine the incident, reflected and transmitted pulse windows used when calculating dynamic material behavior. A number of constraints are presented

which reduce the size of the Hough space searched, and restrict the position and radius of circles used to best fit leading and trailing curvatures of pulses. The automated data analysis approach presented could help to reduce lab-to-lab variability in reported material behavior by unifying the approach used to select pulse windows during analysis, and serves as a possible step forward in standardizing techniques used during Kolsky bar data processing.

Acknowledgements This research was supported by the National Science Foundation CAREER award no. 1847653 and through the Undergraduate Research Opportunities Program (UROP) at the University of Utah awarded to W. Gilliland.

Funding The efforts described here in was supported by the National Science Foundation CAREER under award no. 1847653, and through the Undergraduate Research Opportunities Program (UROP) at the University of Utah.

Availability of Data and Material Raw data will be made available upon reasonable request.

Code Availability Code will be made available through Github and upon reasonable request.

Declarations

Conflict of Interests The authors declare that they have no conflict of interest.

References

1. Hough PVC (1962) Method and means for recognizing complex patterns, December 18 US Patent 3,069
2. Bazin MJ, Benoit JW (1965) Off-line global approach to pattern recognition for bubble chamber pictures. IEEE Trans Nucl Sci 12(4):291–293
3. Duda RO, Hart PE (1972) Use of the hough transformation to detect lines and curves in pictures. Commun ACM 15(1):11–15
4. Maurice C, Fortunier R (2008) A 3d hough transform for indexing ebsd and kossel patterns. J Micro 230(3):520–529
5. Zaefferer S (2007) On the formation mechanisms, spatial resolution and intensity of backscatter kikuchi patterns. Ultramicroscopy 107(2-3):254–266
6. Pourdeyhimi B, Kim HS (2002) Measuring fiber orientation in nonwovens: The hough transform. Text Res J 72(9):803–809
7. Xu B, Yu L (1997) Determining fiber orientation distribution in nonwovens with hough transform techniques. Textile Res J 67(8):563–571
8. Illingworth J, Kittler J (1988) A survey of the hough transform. Comput Vision Graph Image Process 44(1):87–116
9. Leavers VF (1993) Which hough transform? CVGIP: Image Understand 58(2):250–264
10. Mukhopadhyay P, Chaudhuri BB (2015) A survey of hough transform. Pattern Recogn 48(3):993–1010
11. Kimme C, Ballard D, Sklansky J (1975) Finding circles by an array of accumulators. Commun ACM 18(2):120–122
12. Wechsler H, Sklansky J (1977) Automatic detection of ribs in chest radiographs. Pattern Recogn 9(21):30
13. Tsuji S, Matsumoto F (1978) Detection of ellipses by a modified hough transformation. IEEE Comput Archit Lett 27(08):777–781
14. Tsukune H (1983) Extracting elliptical figures from an edge vector field. In: Proceedings conference computer vision and pattern recognition, pp 138–141
15. Merlin PM, Farber DJ (1975) A parallel mechanism for detecting curves in pictures. IEEE Trans Comput 100(1):96–98
16. Ballard DH (1981) Generalizing the hough transform to detect arbitrary shapes. Pattern Recognit 13(2):111–122
17. Kierkegaard P (1992) A method for detection of circular arcs based on the hough transform. Mach Vis Appl 5(4):249–263
18. Pei S-C, Horng J-H (1995) Circular arc detection based on hough transform. Pattern Recognit Lett 16(6):615–625
19. Kolsky H (1949) An investigation of the mechanical properties of materials at very high rates of loading. Proc Phys Soc Sect B 62(11):676
20. Lindholm US, Yeakley LM (1968) High strain-rate testing: Tension and compression. Exp Mech 8(1):1–9
21. Nicholas T (1981) Tensile testing of materials at high rates of strain. Experiment Mechan 21(5):177–185
22. Harding J, Huddart J (1980) The use of the double-notch shear test in determining the mechanical properties of uranium at very high rates of strain. In: Mechanical properties at high rates of strain, 1979
23. Gilat A (2000) Torsional kolsky bar testing. ASM Handbook 8:505–515
24. Gama BA, Lopatnikov SL, Gillespie JW Jr (2004) Hopkinson bar experimental technique: A critical review. Appl Mech Rev 57(4):223–250
25. Gray GT III (2000) Classic split hopkinson pressure bar testing. ASM Handbook 8:462–476
26. Davies EDH, Hunter SC (1963) The dynamic compression testing of solids by the method of the split hopkinson pressure bar. J Mechan Phys Sol 11(3):155–179
27. Chen WW, Bo S (2010) Split Hopkinson (Kolsky) bar: Design, testing and applications. Springer Science & Business Media, New York
28. Casem DT, Grunschel SE, Schuster BE (2011) Interferometric measurement techniques for small diameter kolsky bars. In: Dynamic behavior of materials, vol 1. Springer, pp 463–470
29. Li W, Xu J (2009) Impact characterization of basalt fiber reinforced geopolymeric concrete using a 100-mm-diameter split hopkinson pressure bar. Mater Sci Eng A 513:145–153
30. Song B, Syn CJ, Grupido CL, Chen W, Lu W-Y (2008) A long split hopkinson pressure bar (lshpb) for intermediate-rate characterization of soft materials. Experiment Mechan 48(6):809
31. Lok TS, Li XB, Liu D-S, Zhao PJ (2002) Testing and response of large diameter brittle materials subjected to high strain rate. J Mater Civ Eng 14(3):262–269
32. Lindholm US (1964) Some experiments with the split hopkinson pressure bar. J Mechan Phys Sol 12(5):317–335
33. Follansbee PS, Frantz C (1983) Wave propagation in the split hopkinson pressure bar. J Eng Mater Technol 105:61
34. Li Z, Lambros J (1999) Determination of the dynamic response of brittle composites by the use of the split hopkinson pressure bar. Compos Sci Technol 59(7):1097–1107
35. Francis DK, Whittington WR, Lawrimore WB, Allison PG, Turnage SA, Bhattacharyya JJ (2017) Split hopkinson pressure bar graphical analysis tool. Exp Mech 57(1):179–183
36. Yao Zhenjie, Yi Weidong (2016) Curvature aided hough transform for circle detection. Expert Syst Appl 51:26–33

37. Pătrăucean V, Gurdjos P, Von Gioi RG (2012) A parameterless line segment and elliptical arc detector with enhanced ellipse fitting. In: European conference on computer vision. Springer, pp 572–585
38. Li D, Nan F, Xue T, Yu X (2017) Circle detection of short arc based on randomized hough transform. In: 2017 IEEE International conference on mechatronics and automation (ICMA). IEEE, pp 258–263